Interpretation of enhanced electric dipole transitions in ^{73}Br by the reflection-asymmetric triaxial particle rotor model

Y. Y. Wang [1], Q. B. Chen [2], and S. Q. Zhang [3,*]

[1]*Mathematics and Physics Department, North China Electric Power University, Beijing 102206, China*
[2]*Department of Physics, East China Normal University, Shanghai 200241, China*
[3]*State Key Laboratory of Nuclear Physics and Technology, School of Physics, Peking University, Beijing 100871, China*

(Received 17 January 2022; revised 4 April 2022; accepted 6 April 2022; published 18 April 2022)

The recently observed positive and negative parity bands in ^{73}Br are investigated by the reflection-asymmetric triaxial particle rotor model. The experimental energy spectra as well as the electric transition probabilities $B(E1)$, $B(E2)$, and the ratio $B(E1)/B(E2)$ are well reproduced by the theoretical calculations. It is found that the enhanced interband $E1$ transitions between the opposite-parity bands, a crucial evidence for octupole correlations, are mainly contributed by the intrinsic single-particle electric dipole matrix elements.

DOI: 10.1103/PhysRevC.105.044316

I. INTRODUCTION

As a microscopic quantum many-body system, the nuclear shape provides an intuitive understanding of spatial density distributions of atomic nuclei [1,2], and manifests itself in various exotic nuclear phenomena, such as rotational bands in axially deformed nucleus [1,2], wobbling motion [1] and chiral rotation [3] in triaxially deformed nucleus, and parity doublet partners in pear-shaped nucleus [4,5]. Nowadays, the structure of pear-shaped nucleus has been at the frontiers of both nuclear and particle physics, since it provides a unique probe to test the symmetry violation of charge-parity (CP) beyond the standard model [6]. The study of the pear-shaped nucleus can be traced back to 1950s [7], and it is characterized by the occurrence of, e.g., the interleaved positive and negative parity bands in even-even nuclei, the parity doublet bands in odd-mass nuclei, the enhanced electric dipole ($E1$) and octupole ($E3$) moments, etc. [4,5,8].

The pear shapes of the nucleus can arise from the strong octupole correlations of the nucleons near the Fermi surface occupying states of opposite parity with orbital and total angular momenta differing by $3\hbar$, i.e., $\Delta l = \Delta j = 3\hbar$. Empirically, this condition occurs for proton or neutron particle numbers 34 ($g_{9/2} \leftrightarrow p_{3/2}$), 56 ($h_{11/2} \leftrightarrow d_{5/2}$), 88 ($i_{13/2} \leftrightarrow f_{7/2}$), and 134 ($j_{15/2} \leftrightarrow g_{9/2}$), i.e., when the Fermi surface locates between an intruder orbital and the normal-parity shell [4]. So far, the octupole correlations and the pear-shaped structures have been studied extensively in $A \sim 150$ mass region with $Z \approx 56$ and $N \approx 88$, and in $A \sim 220$ mass region with $Z \approx 88$ and $N \approx 134$, see for reviews [4,5,8].

For the $A \sim 80$ mass region, the availability of an octupole driving pair of $g_{9/2}$ and $p_{3/2}$ orbitals makes it a possible island with strong octupole correlations. Indeed, octupole correlations have been suggested with the observations of strong $E1$ transitions between opposite parity bands, such as in ^{74,78}Se [9,10], ^{78}Br [11], ^{80}Kr [12], ^{81}Rb [13], and ^{83}Y [14]. In particular, the direct lifetime measurements have been performed for several excited states in some nuclei, which allows to obtain the $B(E1)$ strengths in this region. For ^{74}Se, the extracted $B(E1)$ value keeps nearly constant ($\sim 0.017 \times 10^{-4}$ W.u.) from $3\hbar$ to $5\hbar$, whereas for ^{78}Se, it increases from the value 0.017×10^{-4} W.u. for $3\hbar$ to 0.47×10^{-4} W.u. for $7\hbar$. Similar $B(E1)$ values have been reported in three $N = 44$ isotones, i.e., ^{80}Kr ($\sim 0.43 \times 10^{-4}$ W.u.) [12], ^{81}Rb ($\sim 0.50 \times 10^{-4}$ W.u.) [13], and ^{83}Y ($\sim 0.60 \times 10^{-4}$ W.u.) [14], which are one order of magnitude lager than those in ^{74}Se.

Very recently, two strong interconnecting $E1$ transitions between the yrast negative and positive parity bands were reported in ^{73}Br [15], a neighboring odd-A nucleus of ^{74}Se. The lifetime measurements lead to the $B(E1)$ values $\approx 0.46 \times 10^{-4}$ W.u. and $\approx 0.64 \times 10^{-4}$ W.u. for spins $11/2\hbar$ and $15/2\hbar$ in ^{73}Br [15], which are one order of magnitude larger than that observed in the neighboring even-even ^{74}Se. These enhanced $B(E1)$ values indicate the existence of strong octupole correlations in the odd nucleus ^{73}Br. However, it seems that there is no static octupole deformation formed in this nucleus, as the signature partner of the positive parity band was not observed in the level scheme, i.e., the parity doublets are not established. It is therefore of great interest to understand the enhanced $E1$ transitions in ^{73}Br theoretically to have more insight into the octupole correlations in $A \sim 80$ mass region.

Over the past decades, considerable efforts have been devoted to study the collective structures of the nuclei characterized by static and dynamic octupole deformation, such as the quadrupole-octupole collective model [16–26], the interacting boson (or interacting boson-fermion) model [27,28], the reflection asymmetric shell model [29,30], the microscopic core-quasiparticle coupling model [31], the cluster model [32,33], and the reflection-asymmetric particle rotor model [34–36]. For the particle rotor model, a reflection-asymmetric triaxial version (RAT-PRM) [37] has been recently developed

*sqzhang@pku.edu.cn

with both triaxial and octupole degrees of freedom included. This RAT-PRM has been successfully applied to investigate the multiple chiral doublet (MχD) bands with octupole correlations in ^{78}Br [37], ^{131}Ba [38], and ^{124}Cs [39], the octupole collectivities in ^{143}Ba [40], ^{223}Th [41], and ^{79}Se [42], and to explore the novel structure for an ideal chirality-parity (ChP) violation system [43].

In this work, the newly developed RAT-PRM [37] will be applied to investigate the band structures including the energy spectra and electromagnetic transitions observed in ^{73}Br. The model is briefly introduced in Sec. II and the numerical details are presented in Sec. III. The calculated results for the positive and negative parity bands, such as energy spectra and the electromagnetic transitions are discussed in Sec. IV. A summary is given in Sec. V.

II. THEORETICAL FRAMEWORK

The detailed RAT-PRM formalism has been outlined in Ref. [37]. The total Hamiltonian is

$$\hat{H} = \hat{H}^{p(n)}_{\text{intr.}} + \hat{H}_{\text{core}}, \tag{1}$$

where $\hat{H}^{p(n)}_{\text{intr.}}$ is the intrinsic Hamiltonian for valence protons (neutrons) in a reflection-asymmetric triaxially deformed potential, and $\hat{H}_{\text{core}}$ is the Hamiltonian of a reflection-asymmetric triaxial rotor.

The core Hamiltonian $\hat{H}_{\text{core}}$ is generalized straightforwardly from the reflection-asymmetric axial rotor in Ref. [34],

$$\hat{H}_{\text{core}} = \sum_{k=1}^{3} \frac{\hat{R}_k^2}{2\mathcal{J}_k} + \frac{1}{2}E(0^-)(1-\hat{P}_c) \tag{2}$$

with $\hat{R}_k = \hat{I}_k - \hat{j}_{pk} - \hat{j}_{nk}$. Here, $\hat{R}_k$, $\hat{I}_k$, $\hat{j}_{pk}$, and $\hat{j}_{nk}$ are the angular momentum operators for the core, the nucleus, the valence protons, and the valence neutrons, respectively. For the moments of inertia (MoIs), the irrotational flow type $\mathcal{J}_k = \mathcal{J}_0 \sin^2(\gamma - 2k\pi/3)$ is adopted as an approximation [1,2,44]. In the last term, the core parity splitting parameter $E(0^-)$, is treated as a free parameter to describe the excitation energy of the virtual 0^- state [34], and the core parity operator $\hat{P}_c$ is the product of the single-particle parity operator $\hat{\pi}$ and the total parity operator $\hat{P}$.

The intrinsic Hamiltonian $\hat{H}^{p(n)}_{\text{intr.}}$ for valence nucleons is

$$\hat{H}^{p(n)}_{\text{intr.}} = \sum_{\nu>0}\left(\varepsilon^{p(n)}_{\nu} - \lambda\right)(a^{\dagger}_{\nu}a_{\nu} + a^{\dagger}_{\bar{\nu}}a_{\bar{\nu}}) - \frac{\Delta}{2}\sum_{\nu>0}(a^{\dagger}_{\nu}a^{\dagger}_{\bar{\nu}} + a_{\bar{\nu}}a_{\nu}), \tag{3}$$

where λ denotes the Fermi energy, Δ the pairing gap parameter, and $|\bar{\nu}\rangle$ the time-reversal state of $|\nu\rangle$. The single-particle energy $\varepsilon^{p(n)}_{\nu}$ is obtained by diagonalizing a single-particle Hamiltonian $\hat{H}^{p(n)}_{\text{s.p.}}$ that has the form of a Nilsson Hamiltonian [45],

$$\hat{H}^{p(n)}_{\text{s.p.}} = -\tfrac{1}{2}\hbar\omega_0\nabla^2 + V(r,\theta,\varphi) + C\boldsymbol{l}\cdot\boldsymbol{s} + D[\boldsymbol{l}^2 - \langle\boldsymbol{l}^2\rangle_N], \tag{4}$$

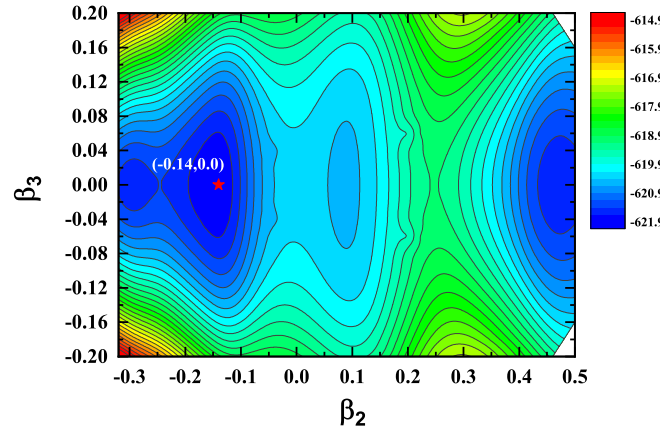

FIG. 1. The potential energy surface of ^{73}Br calculated by the MDC-CDFT approach [48–50]. The contour separation is 0.25 MeV. The pentagram labels the position of the minimum energy.

with the four terms being kinetic energy, the reflection-asymmetric triaxially deformed potential, the spin-orbit term, and the shifting term, respectively. The parameters C and D are related to the standard Nilsson parameters κ and μ with $C = -2\kappa$ and $D = -\kappa\mu$, respectively.

The total Hamiltonian $\hat{H}$ is diagonalized numerically in the symmetrized strong-coupled basis with good parity and angular momentum [37], which gives rise to the eigenvalues and eigenfunctions. With the obtained wave functions the reduced electromagnetic transition probabilities can be calculated [37].

For the electric multipole transition, the corresponding operators contain two terms [1,37],

$$\hat{\mathcal{M}}(E\lambda,\mu) = \hat{q}^{(c)}_{\lambda\mu} + \hat{q}^{(p)}_{\lambda\mu} = \frac{3Ze}{4\pi}R_0^{\lambda}\beta_{\lambda\mu} + e_{\text{eff}}\sum_{i=1}^{n} r_i^{\lambda}Y^*_{\lambda\mu}, \tag{5}$$

which consider the contributions from the core and the valence particles. Here, $R_0 = 1.2A^{1/3}$ fm is the nuclear radius, and e_{eff} is the effective charge. The effective charge e_{eff} in Eq. (5) is introduced for the $E1$ moment to consider the recoil effect of the core and the polarization term caused by the coupling of the dipole mode to the single particle motion [1,37]. For the calculation of the electric quadrupole ($E2$) transitions, the valence particle term in Eq. (5) is neglected since it is much smaller than the term of the core [2].

III. NUMERICAL DETAILS

The deformation parameters in the present RAT-PRM calculation for the positive and negative parity bands in ^{73}Br are based on the microscopic covariant density functional theory (CDFT) calculations [46,48–50] with PC-PK1 [47]. First, the multidimensionally constrained CDFT (MDC-CDFT) [48–50] was performed to obtain the potential energy surface (PES) in the (β_2, β_3) plane. As shown in Fig. 1, the ground state of ^{73}Br is reflection symmetric with $\beta_2 = -0.14$, but the PES around the ground state is very soft

along the direction of β_3, which indicates the strong octupole correlations in ^{73}Br. Another local minimum locates at $\beta_2 = 0.46$ and $\beta_3 = 0$, also with octupole-soft potential. Then, the configuration-fixed triaxial CDFT calculation [46] was performed to obtain the quadrupole deformation parameters (β_2, γ) for the configurations of positive parity band A and negative parity bands B and C in ^{73}Br. The band labels follow the Ref. [15]. The calculated (β_2, γ) for the positive parity configuration $\pi g_{9/2}$ are $(0.47, 6.7^\circ)$, and for the negative parity one $\pi(p_{3/2}f_{5/2})$ are $(0.44, 3.9^\circ)$. In the present RAT-PRM calculations, the deformation parameters $\beta_2 = 0.47$, $\gamma = 6.7^\circ$ and $\beta_3 = 0$ are adopted to give a unified description for the positive and negative parity bands as well as the electromagnetic transitions between them. In order to investigate the effect of the octupole deformation, the RAT-PRM calculations with $\beta_3 = 0.02$ and 0.04 are also performed.

For the intrinsic part, the reflection-asymmetric triaxial Nilsson Hamiltonian (4) with the parameters κ, μ in Ref. [51] is solved in the harmonic oscillator basis [52]. The Fermi energy in Eq. (3) is chosen for proton as $\lambda_p = 43.95$ MeV, corresponding to the $\pi g_{9/2}[\Omega = 3/2]$ orbital. The single-particle space available to the odd nucleon was truncated to 13 levels, with six above and six below the Fermi level. Increasing the size of the single-particle space does not influence the band structure in the present calculations. The pairing gap is taken by the empirical formula $\Delta = 12/\sqrt{A}$ MeV.

For the core part, it turns out to be that a configuration-dependent MoI [39] is necessary to reproduce the experimental energy spectra, which is $\mathcal{J}_0 = 18\ \hbar^2/\text{MeV}$ for positive parity bands and 26 $\hbar^2$/MeV for negative parity bands. The core parity splitting parameter $E(0^-) = 3$ MeV is used.

For the calculations of the electric transition probabilities, the empirical intrinsic dipole moment $Q_{10} = 3/4\pi R_0 Z\beta_{10}$ and quadrupole moment $Q_0 = (3/\sqrt{5\pi})R_0^2 Z\beta_2$ are used with $R_0 = 1.2A^{1/3}$ fm. The dipole deformation parameter β_{10} is obtained by requiring the center of mass coincided with the origin of the coordinate system [37], i.e.,

$$\beta_{10} \approx \frac{18\sqrt{3}}{\sqrt{35\pi}}\beta_2\beta_3\cos\gamma.$$

IV. RESULTS AND DISCUSSION

The energies $E(I)$ calculated by RAT-PRM for the positive parity band A as well as for the negative parity bands B and C are shown in Fig. 2, in comparison with the available data [15]. The calculated energies with positive and negative parity reproduce well the experimental data, except that the calculated energy at spin $37/2\hbar$ for band A overestimates the experimental value by 1.01 MeV. The signature partner of the positive parity band A calculated by the present RAT-PRM is also shown in Fig. 2 labeled as band A′. It can be seen that the signature splitting between bands A and A′ are larger than that between bands B and C, which may explain why the signature partner of band A has not been observed experimentally.

Before studying the interband transitions, we first present the calculated intraband $B(E2)$ values for the positive and negative parity bands in Fig. 3, in comparison with the available data [15]. The calculated $B(E2)$ values slightly increase with

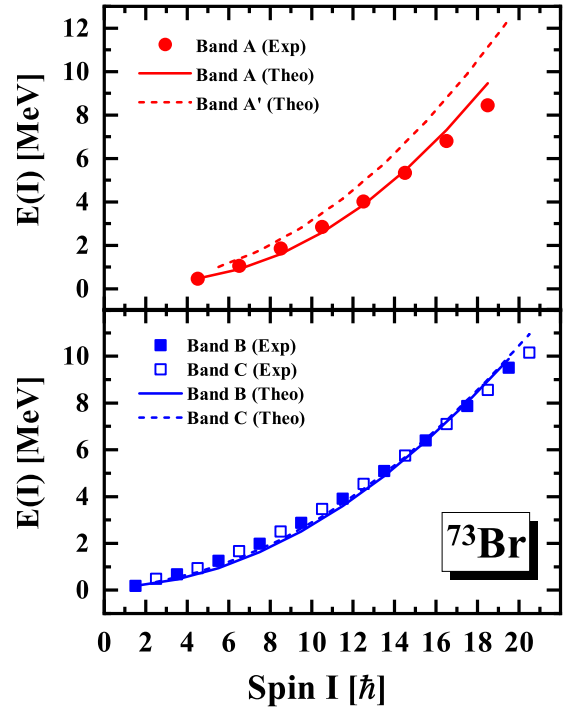

FIG. 2. The energies $E(I)$ for the positive-parity band A as well as for the negative-parity bands B and C in ^{73}Br by RAT-PRM in comparison with the experimental data [15]. The calculated energies are shifted to coincide with the experimental energy at $I = 9/2\hbar$ in band A for positive-parity band and at $I = 3/2\hbar$ in band B for negative-parity bands.

the increase of spin, whereas the experimental ones exhibit a decreasing trend in the observed spin regions, from about 200 W.u. to 100 W.u. for band A and about 150 W.u. to 50 W.u. for bands B and C. As shown in Fig. 3, the calculated $B(E2)$ can reproduce the data reasonably for the spin region $15/2\hbar \leqslant I \leqslant 29/2\hbar$, but fail to reproduce the decreasing trend of the data for the higher spin region, $I \geqslant 31/2\hbar$. This deviation may be attributed to a rigid core adopted in the RAT-PRM, in which the deformation parameters are treated as an input parameter and do not change with spin. This assumption is inconsistent with the rather soft nature of PES shown in Fig. 1. Further efforts on treating the deformation parameters in the RAT-PRM as dynamical variables are necessary to improve the descriptions for the experimental data.

Furthermore, the effects of the quadruple deformation parameters β_2 and γ, as well as the parity splitting parameter $E(0^-)$ on the calculated $B(E2)$ values have been investigated. As shown in Fig. 3(a), the calculated $B(E2)$ values are enhanced about $\pm 20\%$ by changing β_2 by $\pm 10\%$. For the effects of the triaxial deformation γ, as shown in Fig. 3(b), the calculated $B(E2)$ values are similar for $\gamma = 0^\circ$ and $\gamma = 6.7^\circ$ cases, while the $B(E2)$ values are increased by changing γ from 6.7° to 12°. Note that a sudden decrease of the calculated $B(E2)$ value at $33/2\hbar$ in band C for the $\gamma = 12^\circ$ case is found to result from the mixing between $f_{7/2}$ and $(p_{3/2}, f_{5/2})$ components. For the effects of the parameter $E(0^-)$, as shown

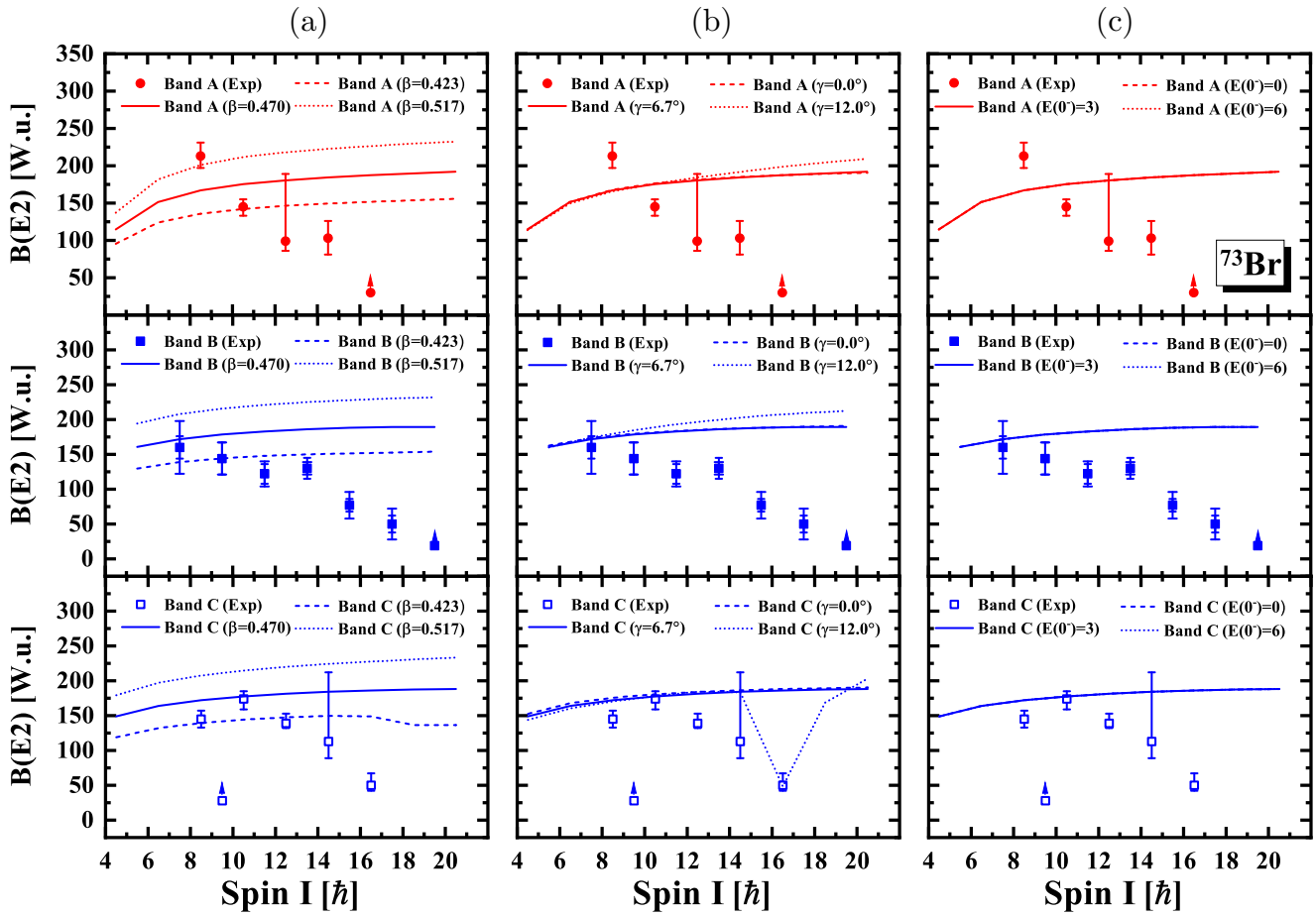

FIG. 3. The intraband $B(E2)$ values for the positive-parity band A as well as for the negative-parity bands B and C in ^{73}Br by RAT-PRM with (a) $\beta_2 = 0.470$, 0.423, and 0.517; (b) $\gamma = 6.7°$, 0°, and 12.0°; (c) $E(0^-) = 3$, 0, and 6 MeV, in comparison with the experimental data [15].

in Fig. 3(c), it is found that the calculated $B(E2)$ values keep nearly unchanged by changing $E(0^-)$ from 0 MeV to 6 MeV.

In Fig. 4, the calculated $B(E1)$ values of the interband $E1$ transitions from band B to band A and the corresponding ratios over the $B(E2)$ values of the intraband $E2$ transitions within band B are shown in comparison with the available data [15]. As is seen, the calculated $B(E1)$ and $B(E1)/B(E2)$ values with $\beta_3 = 0.0$ agree satisfactorily with the experimental data. In order to investigate the effect of the octupole deformation, the results of the RAT-PRM calculations with $\beta_3 = 0.02$ and 0.04 are also shown in Fig. 4. It is found that the $B(E1)$ and the resulting $B(E1)/B(E2)$ ratios depend sensitively on the value of the octupole deformation parameter β_3, which can be enhanced up to about two orders of magnitude by just changing β_3 from 0.0 to 0.04. In contrast, we find that there are no significant influences on the excitation energies and $B(E2)$ values by changing β_3 from 0.02 to 0.04.

The agreement achieved by $\beta_3 = 0.0$ indicates that the $E1$ transitions are mainly from the contribution of the intrinsic valence particle part in Eq. (5). To understand the detailed structures for the observed positive and negative parity bands, the main components of the RAT-PRM wave functions in terms of the strong coupled basis $|IMK\rangle\chi^\nu$ (denoted as $|K, \nu\rangle$ for short) are investigated. Here, $|IMK\rangle$ is the Wigner function with I, M, and K denoting the quantum numbers of the total angular momentum and its projections along the third axis in the laboratory frame and intrinsic frame, and χ^ν represents the intrinsic wave function of the νth proton single-particle level $|\nu\rangle$.

In Table I, the main components of the RAT-PRM wave functions for the positive parity band A in the spin region $9/2\hbar \leqslant I \leqslant 25/2\hbar$, and for the negative parity band B in the spin region $11/2\hbar \leqslant I \leqslant 27/2\hbar$ are shown. It can be seen that the main components for the positive parity band A and negative parity band B are different. The top two components for band A are $|-3/2, 31\rangle$ and $|1/2, 29\rangle$, and for band B are $|1/2, 33\rangle$ and $|1/2, 36\rangle$, respectively. For the positive parity band A, with the spin increasing from $9/2\hbar$ to $25/2\hbar$, the amplitude of the component $|-3/2, 31\rangle$ decreases from 0.82 to 0.67, whereas the component $|1/2, 29\rangle$ increases from 0.53 to 0.68. That is to say, the two components strongly mix each other. For the negative parity band B, the component $|1/2, 33\rangle$ always dominates with the increase of spin for its amplitude changes from 0.94

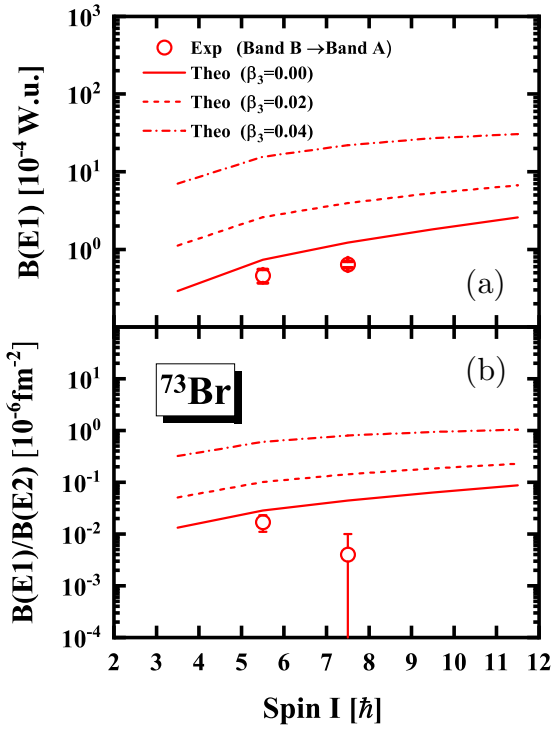

FIG. 4. The calculated $B(E1)$ values for the interband $E1$ transitions from band B to band A and the corresponding ratios over the $B(E2)$ values of the intraband $E2$ transitions (band B) in ^{73}Br in comparison with the available experimental data [15].

TABLE I. The main components expanded in the strong coupled basis $|IMK\rangle\chi^{\nu}$ (denotes as $|K,\nu\rangle$ for short) for the positive-parity band A within spin region $9/2\hbar \leqslant I \leqslant 25/2\hbar$, and for the negative-parity band B within spin region $11/2\hbar \leqslant I \leqslant 27/2\hbar$. The I, M, K denote the quantum numbers of the total angular and its projection along the third axis in the laboratory frame and intrinsic frame, respectively. The χ^{ν} represent the intrinsic wave functions that obtained by diagonalizing the reflection-asymmetric triaxial Nilsson Hamiltonian.

I^{π}	Main components in terms of $\|K,\nu\rangle$
Band A	
$9/2^+$	$+0.82\|-\frac{3}{2},31\rangle+0.53\|\frac{1}{2},29\rangle+0.18\|\frac{5}{2},42\rangle+\cdots$
$13/2^+$	$+0.76\|-\frac{3}{2},31\rangle+0.60\|\frac{1}{2},29\rangle+0.21\|\frac{5}{2},42\rangle+\cdots$
$17/2^+$	$-0.72\|-\frac{3}{2},31\rangle-0.64\|\frac{1}{2},29\rangle-0.22\|\frac{5}{2},42\rangle+\cdots$
$21/2^+$	$+0.69\|-\frac{3}{2},31\rangle+0.67\|\frac{1}{2},29\rangle+0.23\|\frac{5}{2},42\rangle+\cdots$
$25/2^+$	$+0.68\|\frac{1}{2},29\rangle+0.67\|-\frac{3}{2},31\rangle+0.24\|\frac{5}{2},42\rangle+\cdots$
Band B	
$11/2^-$	$-0.94\|\frac{1}{2},33\rangle-0.27\|\frac{1}{2},36\rangle+0.12\|-\frac{3}{2},36\rangle+\cdots$
$15/2^-$	$+0.93\|\frac{1}{2},33\rangle+0.26\|\frac{1}{2},36\rangle-0.14\|-\frac{3}{2},36\rangle+\cdots$
$19/2^-$	$+0.92\|\frac{1}{2},33\rangle+0.26\|\frac{1}{2},36\rangle-0.15\|-\frac{3}{2},36\rangle+\cdots$
$23/2^-$	$-0.91\|\frac{1}{2},33\rangle-0.25\|\frac{1}{2},36\rangle+0.16\|-\frac{3}{2},36\rangle+\cdots$
$27/2^-$	$+0.90\|\frac{1}{2},33\rangle+0.25\|\frac{1}{2},36\rangle-0.16\|-\frac{3}{2},36\rangle+\cdots$

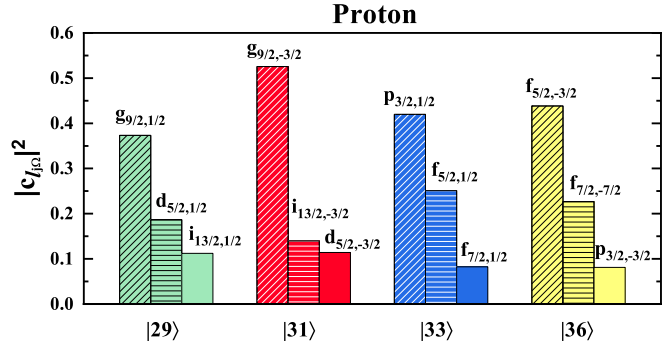

FIG. 5. The main components $l_{j\Omega}$ of the proton single particle levels $|\nu\rangle$ with $\nu = 29, 31, 33$, and 36.

to 0.90. We further study the main spherical harmonic oscillator components $l_{j\Omega}$ for these proton single particle levels, as shown in Fig. 5. Since $\beta_3 = 0.0$ in the present calculation, the parity is a good quantum number, i.e., the spherical components with opposite parity can not mix. For the positive parity levels $|31\rangle$ and $|29\rangle$ mainly contributed to band A, their dominate components are the same $g_{9/2}$ orbital but with different Ω values, $\Omega = 3/2$ and $1/2$, respectively. Besides the $g_{9/2}$ orbital, there are also some $d_{5/2}$ and $i_{13/2}$ components mixed in these two levels. For the negative parity level $|33\rangle$ mainly contributed to band B, its dominate component is $p_{3/2}$ with $\Omega = 1/2$, and which is mixed with some $f_{5/2}$ and $f_{7/2}$ components.

Based on the intrinsic band structure of bands A and B, further study of the enhance $E1$ transitions observed between these two bands can be performed. As mentioned above, the $E1$ transitions from band B to band A are mainly from the contribution of the intrinsic valence particle part in Eq. (5), i.e., $\sim|\langle K',\nu'|rY_{10}|K,\nu\rangle|^2$. In fact, in order to obtain nonzero $E1$ single-particle matrix elements, one needs the intrinsic components of band A and B satisfy the condition of $\Delta K = 0$, $\Delta l = \Delta j = 1$, and $\Delta\Omega = 0$. Following this condition, one can conclude from the components presented in Table I and Fig. 5 that the enhanced $E1$ transitions between bands A and B mainly result from the matrix elements between components $g_{9/2}[\Omega = 1/2]$ in band A and $f_{7/2}[\Omega = 1/2]$ in band B, and between $d_{5/2}[\Omega = 1/2]$ in band A and $p_{3/2}[\Omega = 1/2]$ in band B.

V. SUMMARY

In summary, based on the combination of the microscopic MDC-CDFT, the triaxial CDFT, and RAT-PRM, the recently observed positive and negative parity bands in ^{73}Br have been studied. The obtained soft nature of PES with respect to β_3 from MDC-CDFT supports the octupole correlations in this nucleus. Based on the configuration and the deformation parameters from triaxial CDFT, the RAT-PRM calculation has been performed. The calculated energy spectra, $B(E2)$, $B(E1)$, and the ratio $B(E1)/B(E2)$ reproduce reasonably the available experimental data. By analyzing the main components of the RAT-PRM wave functions, it is found that the

interband $E1$ transition probabilities, the crucial evidence for the octupole correlations, between the opposite parity bands are mainly contributed by the intrinsic single-particle electric dipole matrix elements between components $g_{9/2}[\Omega = 1/2]$ and $f_{7/2}[\Omega = 1/2]$, and between $d_{5/2}[\Omega = 1/2]$ and $p_{3/2}[\Omega = 1/2]$. Nevertheless, further investigation of the effects of other octupole degrees of freedom, such as β_{32} and β_{33}, for the octupole collectivity deserves to be performed.

ACKNOWLEDGMENTS

This work was partly supported by the National Natural Science Foundation of China (NSFC) under Grants No. 11875075 and No. 11935003, the National Key R&D Program of China (2018YFA04044000), the Deutsche Forschungsgemeinschaft (DFG) and the NSFC through funds provided to the Sino-German CRC110 "Symmetries and the Emergence of Structure in QCD" (DFG Grant No. TRR110 and NSFC Grant No. 12070131001).

[1] A. Bohr and B. R. Mottelson, *Nuclear Structure* (Benjamin, New York, 1975), Vol. II.
[2] P. Ring and P. Schuck, *The Nuclear Many-Body Problem* (Springer-Verlag, Berlin, 1980).
[3] S. Frauendorf and J. Meng, Nucl. Phys. A **617**, 131 (1997).
[4] P. A. Butler and W. Nazarewicz, Rev. Mod. Phys. **68**, 349 (1996).
[5] P. A. Butler, J. Phys. G: Nucl. Part. Phys. **43**, 073002 (2016).
[6] L. P. Gaffney, P. A. Butler, M. Scheck, A. B. Hayes, F. Wenander, M. Albers, B. Bastin, C. Bauer, A. Blazhev, S. Bönig *et al.*, Nature **497**, 199 (2013).
[7] F. S. Stephens, F. Asaro, and I. Perlman, Phys. Rev. **96**, 1568 (1954).
[8] P. A. Butler, Proc. R. Soc. A **476**, 20200202 (2020).
[9] R. Schwengner, G. Winter, J. Döring, L. Funke, P. Kemnitz, E. Will, A. E. Sobov, A. D. Efimov, M. F. Kudojarov, I. Kh. Lemberg *et al.*, Z. Phys. A **326**, 287 (1987).
[10] J. Adam, M. Honusek, A. Špalek, D. N. Doynikov, A. D. Efimov, M. F. Kudojarov, I. Kh. Lemberg, A. A. Pasternak, O. K. Vorov, and U. Y. Zhovliev, Z. Phys. A **332**, 143 (1989).
[11] C. Liu, S. Y. Wang, R. A. Bark, S. Q. Zhang, J. Meng, B. Qi, P. Jones, S. M. Wyngaardt, J. Zhao, C. Xu, S. G. Zhou, S. Wang, D. P. Sun, L. Liu, Z. Q. Li, N. B. Zhang, H. Jia, X. Q. Li, H. Hua, Q. B. Chen, Z. G. Xiao, H. J. Li, L. H. Zhu, T. D. Bucher, T. Dinoko, J. Easton, K. Juhasz, A. Kamblawe, E. Khaleel, N. Khumalo, E. A. Lawrie, J. J. Lawrie, S. N. T. Majola, S. M. Mullins, S. Murray, J. Ndayishimye, D. Negi, S. P. Noncolela, S. S. Ntshangase, B. M. Nyako, J. N. Orce, P. Papka, J. F. Sharpey-Schafer, O. Shirinda, P. Sithole, M. A. Stankiewicz, and M. Wiedeking, Phys. Rev. Lett. **116**, 112501 (2016).
[12] L. Funke, J. Döring, F. Dubbers, P. Kemnitz, E. Will, G. Winter, V. G. Kiptilij, M. F. Kudojarov, I. Kh. Lemberg, A. A. Pasternak *et al.*, Nucl. Phys. A **355**, 228 (1981).
[13] J. Döring, R. Schwengner, L. Funke, H. Rotter, G. Winter, B. Cederwall, F. Lidén, A. Johnson, A. Atac, J. Nyberg, and G. Sletten, Phys. Rev. C **50**, 1845 (1994).
[14] F. Cristancho, C. J. Gross, K. P. Lieb, D. Rudolph, Ö. Skeppstedt, M. A. Bentley, W. Gelletly, H. G. Price, J. Simpson, J. L. Durell *et al.*, Nucl. Phys. A **540**, 307 (1992).
[15] S. Bhattacharya, T. Trivedi, D. Negi, R. P. Singh, S. Muralithar, R. Palit, I. Ragnarsson, S. Nag, S. Rajbanshi, M. K. Raju, V. V. Parkar, G. Mohanto, S. Kumar, D. Choudhury, R. Kumar, R. K. Bhowmik, S. C. Pancholi, and A. K. Jain, Phys. Rev. C **100**, 014315 (2019).
[16] P. G. Bizzeti and A. M. Bizzeti-Sona, Phys. Rev. C **70**, 064319 (2004).
[17] P. G. Bizzeti and A. M. Bizzeti-Sona, Phys. Rev. C **77**, 024320 (2008).
[18] P. G. Bizzeti and A. M. Bizzeti-Sona, Phys. Rev. C **81**, 034320 (2010).
[19] P. G. Bizzeti and A. M. Bizzeti-Sona, Phys. Rev. C **88**, 011305(R) (2013).
[20] D. Bonatsos, D. Lenis, N. Minkov, D. Petrellis, and P. Yotov, Phys. Rev. C **71**, 064309 (2005).
[21] N. Minkov, P. Yotov, S. Drenska, W. Scheid, D. Bonatsos, D. Lenis, and D. Petrellis, Phys. Rev. C **73**, 044315 (2006).
[22] N. Minkov, S. Drenska, M. Strecker, and W. Scheid, J. Phys. G: Nucl. Part. Phys. **36**, 025108 (2009).
[23] N. Minkov, S. Drenska, M. Strecker, W. Scheid, and H. Lenske, Phys. Rev. C **85**, 034306 (2012).
[24] N. Minkov, Phys. Scr. **T154**, 014017 (2013).
[25] N. Minkov and A. Pálffy, Phys. Rev. Lett. **118**, 212501 (2017).
[26] A. Dobrowolski, K. Mazurek, and A. Góźdź, Phys. Rev. C **94**, 054322 (2016).
[27] N. V. Zamfir and D. Kusnezov, Phys. Rev. C **63**, 054306 (2001).
[28] C. Alonso, J. Arias, A. Frank, H. Sofia, S. Lenzi, and A. Vitturi, Nucl. Phys. A **586**, 100 (1995).
[29] Y. S. Chen and Z. C. Gao, Phys. Rev. C **63**, 014314 (2000).
[30] Y.-J. Chen, Z.-C. Gao, Y.-S. Chen, and Y. Tu, Phys. Rev. C **91**, 014317 (2015).
[31] W. Sun, S. Quan, Z. P. Li, J. Zhao, T. Nikšić, and D. Vretenar, Phys. Rev. C **100**, 044319 (2019).
[32] T. Shneidman, G. Adamian, N. Antonenko, R. Jolos, and W. Scheid, Phys. Lett. B **526**, 322 (2002).
[33] G. G. Adamian, N. V. Antonenko, R. V. Jolos, and T. M. Shneidman, Phys. Rev. C **70**, 064318 (2004).
[34] G. A. Leander and R. K. Sheline, Nucl. Phys. A **413**, 375 (1984).
[35] G. A. Leander and Y. S. Chen, Phys. Rev. C **35**, 1145 (1987).
[36] G. A. Leander and Y. S. Chen, Phys. Rev. C **37**, 2744 (1988).
[37] Y. Y. Wang, S. Q. Zhang, P. W. Zhao, and J. Meng, Phys. Lett. B **792**, 454 (2019).
[38] Y. P. Wang, Y. Y. Wang, and J. Meng, Phys. Rev. C **102**, 024313 (2020).
[39] Y. Y. Wang and S. Q. Zhang, Phys. Rev. C **102**, 034303 (2020).
[40] C. Morse, A. O. Macchiavelli, H. L. Crawford, S. Zhu, C. Y. Wu, Y. Y. Wang, J. Meng, B. B. Back, B. Bucher, C. M. Campbell, M. P. Carpenter, J. Chen, R. M. Clark, M. Cromaz, P. Fallon, J. Henderson, R. V. F. Janssens, M. D. Jones, T. L. Khoo, F. G. Kondev, T. Lauritsen, I. Y. Lee, J. Li, D. Potterveld, C. Santamaria, G. Savard, D. Seweryniak, S. Stolze, and D. Weisshaar, Phys. Rev. C **102**, 054328 (2020).

[41] Y. Y. Wang, Phys. Rev. C **104**, 014318 (2021).
[42] S. Rajbanshi, R. Palit, R. Raut, Y. Y. Wang, Z. X. Ren, J. Meng, Q. B. Chen, S. Ali, H. Pai, F. S. Babra, R. Banik, S. Bhattacharya, S. Bhattacharyya, P. Dey, S. Malik, G. Mukherjee, M. S. R. Laskar, S. Nandi, R. Santra, T. Trivedi, S. S. Ghugre, and A. Goswami, Phys. Rev. C **104**, 064316 (2021).
[43] Y. Y. Wang, X. H. Wu, S. Q. Zhang, P. W. Zhao, and J. Meng, Sci. Bull. **65**, 2001 (2020).
[44] M. G. Davidson, Phys. Rev. C **2**, 1814 (1970).
[45] S. G. Nilsson, Mat. Fys. Medd. Dan. Vid. Selsk **29**, 16 (1955).
[46] J. Meng, J. Peng, S. Q. Zhang, and S.-G. Zhou, Phys. Rev. C **73**, 037303 (2006).
[47] P. W. Zhao, Z. P. Li, J. M. Yao, and J. Meng, Phys. Rev. C **82**, 054319 (2010).
[48] B. N. Lu, E. G. Zhao, and S. G. Zhou, Phys. Rev. C **85**, 011301(R) (2012).
[49] J. Zhao, B. N. Lu, E. G. Zhao, and S. G. Zhou, Phys. Rev. C **86**, 057304 (2012).
[50] B. N. Lu, J. Zhao, E. G. Zhao, and S. G. Zhou, Phys. Rev. C **89**, 014323 (2014).
[51] S. G. Nilsson, C. F. Tsang, A. Sobiczewski, Z. Szymański, S. Wycech, C. Gustafson, I.-L. Lamm, P. Möller, and B. Nilsson, Nucl. Phys. A **131**, 1 (1969).
[52] Y. Y. Wang and Z. X. Ren, Sci. China Phys. Mech. Astron. **61**, 082012 (2018).